Journal of Molecular Structure 1163 (2018) 316–326

Contents lists available at ScienceDirect

Journal of Molecular Structure

journal homepage: http://www.elsevier.com/locate/molstruc

Investigation of non-covalent and hydrogen bonding interactions on the formation of crystalline networks and supramolecular synthons of a series of α-aminophosphonates: Crystallography and DFT studies

Masoud Mirzaei*, Hossein Eshghi, Fateme Akhlaghi Bagherjeri, Mahdi Mirzaei, Abolghasem Farhadipour

Department of Chemistry, Faculty of Science, Ferdowsi University of Mashhad, Mashhad, Iran

ARTICLE INFO

Article history:
Received 19 January 2018
Received in revised form
4 March 2018
Accepted 6 March 2018
Available online 7 March 2018

Keywords:
α-aminophosphonates
X-ray diffraction
Supramolecular synthon
Non-covalent interactions
Unconventional interactions
Theoretical studies

ABSTRACT

α-Aminophosphonates have been rarely explored in the field of crystal engineering. These organic molecules are capable of forming reliable and reproducible supramolecular synthons through non-covalent interactions that can be employed for designing high dimensional supramolecular architectures. Here, we systematically study the influence of conventional and unconventional hydrogen bonding interactions on the formation of these synthons and stability of the crystal packing. The theoretical studies were employed to further confirm the presence of these synthons by comparing the stabilization energies of the dimers and monomers. The dependence of the stability of NH···O hydrogen bonds to the aromatic substituents were investigated using NBO analysis. The most stable compound was determined by comparing the HOMO-LUMO energy gap of all compounds and compared with NBO analysis.

1. Introduction

The understanding of intermolecular interactions in the crystal packing and utilizing this knowledge to design supramolecular networks such as ribbon, sheets, channels and *etc.*, with desired physical and chemical properties is the ultimate goal of crystal engineering. The crystal engineering of organic molecules *via* intermolecular interactions is considered as a new organic synthesis (supramolecular) versus traditional organic synthesis (molecular) using covalent bonds [1]. To rationalize the design of new supramolecular structures, non-covalent interactions including hydrogen bonds [2–6], the π–π stacking [7–10] anion/Lp···π [11–19], and halogen bonds [20–24] play important roles in the prediction of the orientation of the molecules in the solid. In this regard, the role of directional conventional O/NH···O and unconventional C–H···O/N, C–H···π and O/N–H···π hydrogen bonds has been very well recognized in different fields related to biological, pharmacological, chemical, physical, and materials sciences [2,3,5,25–27]. These interactions can be combined by a designed placement of functional groups in the molecular skeleton to generate *supramolecular synthons* [1,28,29]. The recognition of characteristic synthons of different functional groups in the packing is crucial for analysing the more complex crystal packings and designing novel supramolecular structures. In fact, the goal of crystal engineering is to identify and design synthons that maintain intact from one network structure to another, which ensures generality and predictability [30–33].

α-Aminophosphonic acids are structural analogous of natural α-amino acids in which the carboxilic group is replaced by phosphonic group resulting in the presence of the characteristic N–C–P scaffold (Scheme 1) [34–36]. These compounds are considerable interest because of their existance in many living organisms and their biological activity as inhibitors of various enzymes (metalloenzymes) having amino acid substrates [37,38]. These compounds contain amine and phosphonate functional groups capable of either acting as a ligand to provide distinct complexing [39–42] and pharmacological [43–46] properties or participating in non-covalent interactions such as different types of H bonds. The identification of these intermolecular interactions involving amine and phosphonate functional groups can shed light on their essential roles in corresponding biological processes such as interacting

* Corresponding author.
E-mail address: mirzaeesh@um.ac.ir (M. Mirzaei).

https://doi.org/10.1016/j.molstruc.2018.03.014
0022-2860/

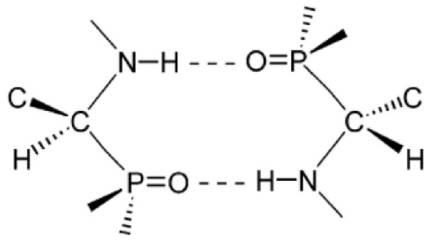

Scheme 1. The characteristic synthon of α-aminophosphonates, $R_2^2(10)$, forming *via* arrangement of two antiparallel hydrogen bonds of phosphonate and amine functional groups.

with DNA or drug design [37,38,43,47–49]. In addition, the non-covalent interactions between functional groups of α-aminophosphonates bearing aromatic rings confer reliable and ubiquitous characteristic supramolecular synthons (Scheme 1) which has not featured prominently in crystal engineering applications to date [50]. For the first time, Rao has advocated the potential role of this directional supramolecular synthon in transformation of open-framework metal phosphates from one-dimensional ladder or chain to higher dimensional structures in presence of amine [51]. There are other organic molecules containing amine and phosphoric groups including C(O)NHP(O)-based phosphoric triamide structures which is expected to display similar (but not identical) synthons as α-aminophosphonic acids (esters) studied by Vahdani et al.very recently [52].

We previously synthesized a series of α-aminophosphonate esters under catalyst- and solvent-free conditions which revealed significant anticancer properties (Scheme 2) [53]. It was realized that there is not a comprehensive study on the influence of the non-covalent interactions on the formation and stability of the supramolecular structures and recognition of the typical synthons of this family of organic molecules. Thus, we decided to systematically investigate the different types of non-covalent interactions inside the packing and explore all the molecular recognition features that lead to the supramolecular synthons and ultimately compare these findings with the theoretical results.

2. Experimental

2.1. X-ray crystallography instrument

All compounds were dissolved in a mixture of EtOAC/n-Hexane (1:4) solvents and left for slow evaporation. The crystallographic data (Table 1) were collected on Bruker APEX-Duo (**4a**), APEX-II (**4e**) and Rigaku MicroMax-007HF (**4b-4d**, **4f** and **4h**) diffractometers using Quazar MX Multilayer Optics (**4a**), Confocal Max Flux optic (**4b**), graphite (**4e**) monochromated Mo-Kα radiation (0.71073 Å). Emperical **(4a-4d** and **4f-4h**) and multi scan (**4e**) absorption corrections were carried. All structures were solved by Sir2011 program [54] except **4e** (SHELXS97) [55] and refined by the full-matrix least-squares method on $|F|^2$ using the SHELXL-2014 [56] (SHELXL97 [57] for **4e**) crystallographic package. All non-hydrogen atoms were refined anisotropically. Disorder refinement models were applied to the carbon and hydrogen atoms of one or more ethyl groups in compounds **4a**, **4b**, **4c**, **4f** and **4h** as well as one phenyl ring of **4a** with the aid of SUMP instruction in order to assign independently site occupancy factors (s.o.f.s) to the disordered atoms (Fig. S1). DFIX restraints were used to model all the disordered ethyl fragments.

2.2. Computational details

Density functional theory (DFT) calculations were carried out using the Gaussian 09 program [58]. The B3LYP/6-311G(d,p) level of theory was used to optimize the geometry of the molecule. Additionally, a natural bond orbital (NBO) analysis was performed at the B3LYP level of theory and with the 6-311G(d,p) basis set using the NBO package [59] included in the Gaussian 09 Program. Similar to our previous work, to calculate the HOMO-LUMO and hydrogen bond energies in these structures, a hydrogen bonded cluster (dimer) of two molecules was constructed and used as the input file for the calculation set up [60,61]. This assembly is similar to the 'Display Options' of the Mercury program [62] after selecting the ″H-Bond″ and ″expand all″ options, which includes two N–H···O interactions.

3. Results and discussion

3.1. Crystal structure analysis

The molecular views and atoms numbering schemes of all compounds (**4a-h**) are included in Fig. 1. The asymmetric units of structures **4b**, **4c** and **4e-4h** are consist of one molecule, while compounds **4a** and **4d** contain two independent molecules in their asymmetric units with the primary difference between the two being opposite configurations about the central chiral carbon (Cα) atom. Each three-component molecule comprised of two aromatic rings in which one of them derives from aniline precursor with different substituents (**4a** (*p*-Cl), **4b** (*p*-Me), **4c** (*m*-Me), **4d** (*p*-OMe), **4e** (*p*-Br), **4f** (*m*-Me) and **4h** (2-aminobenzothiazol) and the other one stems from the benzaldehyde precursor substituted by diethylamine (**4a-4d**) or dimethylamine (**4e-4h**) attached to the diethyl phosphite group (Fig. 1).

The P atom has a distorted tetrahedral environment in all compounds involving two O-ethyl groups, one Cα atom, and a double bond with O atom with bond angles at the range of 99.9(1)-116.97(6)° [35,36]. The benzene ring with the conjunction N atom surrounded by one hydrogen and two carbon atoms at the range of 110(1)-120.9(3)° is fairly planar (Table S1) [63,64]. Despite differing

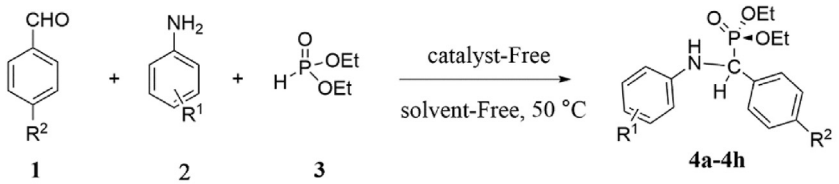

R^2= 4-N(Et)$_2$(**4a-4d**), 4-N(CH$_3$)$_2$ (**4e-4h**)

R^1=*p*-Cl (**4a**), *p*-Me (**4b**), *m*-Me (**4c**, **4f**), *p*-Br (**4e**), *p*-OCH$_3$ (**4d**), 2-aminobenzothiazole (**4h**)

Scheme 2. Catalyst-free and solvent-free coupling of benzaldehydes and anilines with diethyl phosphite for synthesis of α-aminophosphonates [53].

Table 1
Crystal data and structure-refinement parameters for **4a-4h**.

	4a	4b	4c	4d	4e	4f	4h
Formula	$C_{21}H_{30}ClN_2O_3P$	$C_{22}H_{33}N_2O_3P$	$C_{22}H_{33}N_2O_3P$	$C_{22}H_{33}N_2O_4P$	$C_{19}H_{26}BrN_2O_3P$	$C_{20}H_{29}N_2O_3P$	$C_{20}H_{26}N_3O_3PS$
M_r	404.47	404.47	404.47	420.47	441.30	376.42	419.47
Crystal system	Monoclinic	Triclinic	Triclinic	Triclinic	Triclinic	Triclinic	Triclinic
Space group	$P2_1/c$	$P\bar{1}$	$P\bar{1}$	$P\bar{1}$	$P\bar{1}$	$P\bar{1}$	$P\bar{1}$
T/K	293(2)	100(2)	100(2)	100(2)	296(2)	100(2)	100(2)
a/Å	16.972(3)	9.3421(10)	9.419(3)	10.635(2)	10.0113(4)	8.5398(6)	8.3642(3)
b/Å	14.091(2)	11.2430(13)	11.160(2)	12.774(3)	10.2573(4)	10.8039(13)	11.4747(8)
c/Å	21.262(3)	12.4962(12)	11.782(2)	18.246(3)	10.6974(5)	12.0212(13)	12.1918(9)
α/°	–	104.6324(17)	65.765(19)	94.099(4)	69.219(2)	87.520(9)	87.617(8)
β/°	111.179(5)	101.5141(13)	76.44(2)	101.8135(15)	81.112(2)	71.921(7)	71.952(6)
γ/°	–	112.1076(19)	80.30(3)	111.746(4)	69.730(2)	74.624(8)	71.725(6)
V/Å^3	4741.6(13)	1111.0(2)	1094.1(5)	2223.8(7)	1052.81(7)	1015.70(19)	1054.43(12)
Z	8	2	2	4	2	2	2
ρ_{calcd}/g cm^{-3}	1.190	1.209	1.228	1.256	1.392	1.231	1.321
F(000)	1808	436	436	904	456	404	444
R_1 [$I > 2\sigma(I)$]	0.0871	0.0444	0.0832	0.0411	0.0448	0.0402	0.0341
wR_2 [$I > 2\sigma(I)$]	0.2699	0.1240	0.2047	0.1106	0.1242	0.1192	0.0973
R_1 (all data)	0.1266	0.0474	0.1041	0.0492	0.0579	0.0442	0.0379
wR_2 (all data)	0.3284	0.1264	0.2117	0.1131	0.1349	0.11215	0.0986
GOF	1.040	1.027	0.914	1.062	0.999	1.096	1.086

in the orientations of the ethoxy groups of the phosphonate and aromatic substituents, in all compounds the central {HCα–P=O} moiety has the hydrogen and oxygen atoms trans to one another.

The P=O bond lengths of all compounds except compound **4a** are slightly longer than the phosphorus-oxygen double bond length (1.45 Å). Moreover, the Cα –P and Cα –N bond lengths are almost comparable with similar structures [65] and in the narrow ranges 1.804(5) – 1.833(3) Å and 1.450(2) – 1.474(2) Å, respectively, with no particular correlation with the identities of the substituents on the central carbon atom (Table S2).

Variety of hydrogen-bond patterns are observed due to the presence of the O=P group with the possibility of acting as a simple, double or even triple hydrogen-bond acceptor and/or due to the involvement of the π-system or halogen atom as other acceptor groups taking part in the hydrogen bond pattern. The most prominent feature of these supramolecular structures is the supramolecular synthon R_2^2 (10) [64,66,67] comprised of hydrogen-bonded dimers formed through non-parallel N_{cc}–H…O=P hydrogen bonds which repeats in all structures (Table 2). For **4a** and **4d**, the dimer is formed between the two independent molecules in the asymmetric units while for the remaining the dimers are formed across the centers of symmetry (Figs. 2–8). These strong hydrogen bonds accompanying unconventional CH···O=P, CH···Cl [63] and CH … π [68,69] (Table 2) hydrogen bonds play essential roles in the formation and stability of the crystalline materials. The details of these non-covalent interactions for each of compounds **4a-4h** will be discussed separately.

In addition of synthon R_2^2 (10), the R_2^1 (6) and R_2^1 (7) synthons are also form through N_{cc}H … O … C_{cc}H hydrogen bonds in which the oxygen of phosphonate group acts as a double acceptor (bifurcated hydrogen bond). These dimers further connect to the adjacent dimers *via* (aromatic and aliphatic) CH … π hydrogen bonds along *a* and *c* axis. These 2D sheets are extended through unconventional CH···Cl hydrogen bonds forming chain motif C_1^1 (12) along *b* axis to give a 3D supramolecular network (Fig. 2).

In structure **4b**, similar to **4a** each dimer connects to each other *via* N_{cc}H … O=P hydrogen bonds along *c* axis to create R_2^2 (10) synthon. However, the oxygen of the phosphonate group participates in a bifurcated hydrogen bond through the (aliphatic) CH···O=P of the third molecule and NH···O=P of the dimer. The CH···O=P and CH … π hydrogen bonds along *a* axis accompanying strong NH···O=P hydrogen bonds generate a 2D supramolecular network (Fig. 3).

The trifurcated hydrogen bonds form *via* the interactions between the hydrogen atoms of NH and two (aromatic) CH with oxygen of phosphonate groups along *b* axis in compound **4c**. These hydrogen bonds create dimers which are stabilized through generation of five synthons as one R_2^2 (10), two R_2^1 (6) and two R_2^1 (7). Furthermore, the (aliphatic) CH … π hydrogen bonds along *c* axis extend this 2D supramolecular network (Fig. 4).

In compound **4d,** the bifurcated hydrogen bonds are observed from three-centered N_{cc}H … O … C_{cc}H creating R_2^2 (10) and two R_2^1 (6) along *a* axis. In addition, the aromatic ring *Cg*1 is exposed to the three aliphatic CH groups and takes part in three CH … π hydrogen bonds which further stabilizes the 3D supramolecular network (Fig. 5).

The synthons observed in the crystal packing of **4e** extended along *b* axis is similar to **4d** which connect the dimers. These dimers are further stabilized *via* (aromatic) CH … π hydrogen bonds in the same axis to form 1D chain (Fig. 6).

Trifurcated hydrogen bonds form *via* the interactions between hydrogen atoms of NH and two (aromatic) CH with oxygen of phosphonate groups along *c* axis in compound **4f** to creat five synthons similar to **4c**. Moreover, unconventional CH … π hydrogen bonds extended along *b* and *a* axes construct a 3D supramolecular network (Fig. 7).

Compound **4h** contains a different aromatic ring on the amine fragment compared to the other compounds in which an aromatic five-member ring (C3NS) is attached to a phenyl ring [68]. It is worth noting that in addition of the synthon R_2^2 (10), two five-member rings, R(5), formed *via* the interaction of S atom and the oxygen of phosphonate group accompanying the strong NH···O=P hydrogen bond connect the dimer along *b* axis. The interatomic distance of S and O atoms (3.171 Å) is shorter than the sum of their van der Waals radii (3.27 Å). Furthermore, two different CH … π hydrogen bonds are possible due to the presence of five-member and six-member rings along *a* and *c* axis, respectively, giving rise to a 3D supramolecular network.

3.2. Theoretical studies

3.2.1. Optimized structures

The optimized geometry parameters corresponded to the hydrogen bonds are summarized in Table 3. The average values of N–H bond lengths for the hydrogen bonded cluster of all structures are relatively longer than the corresponding monomer values

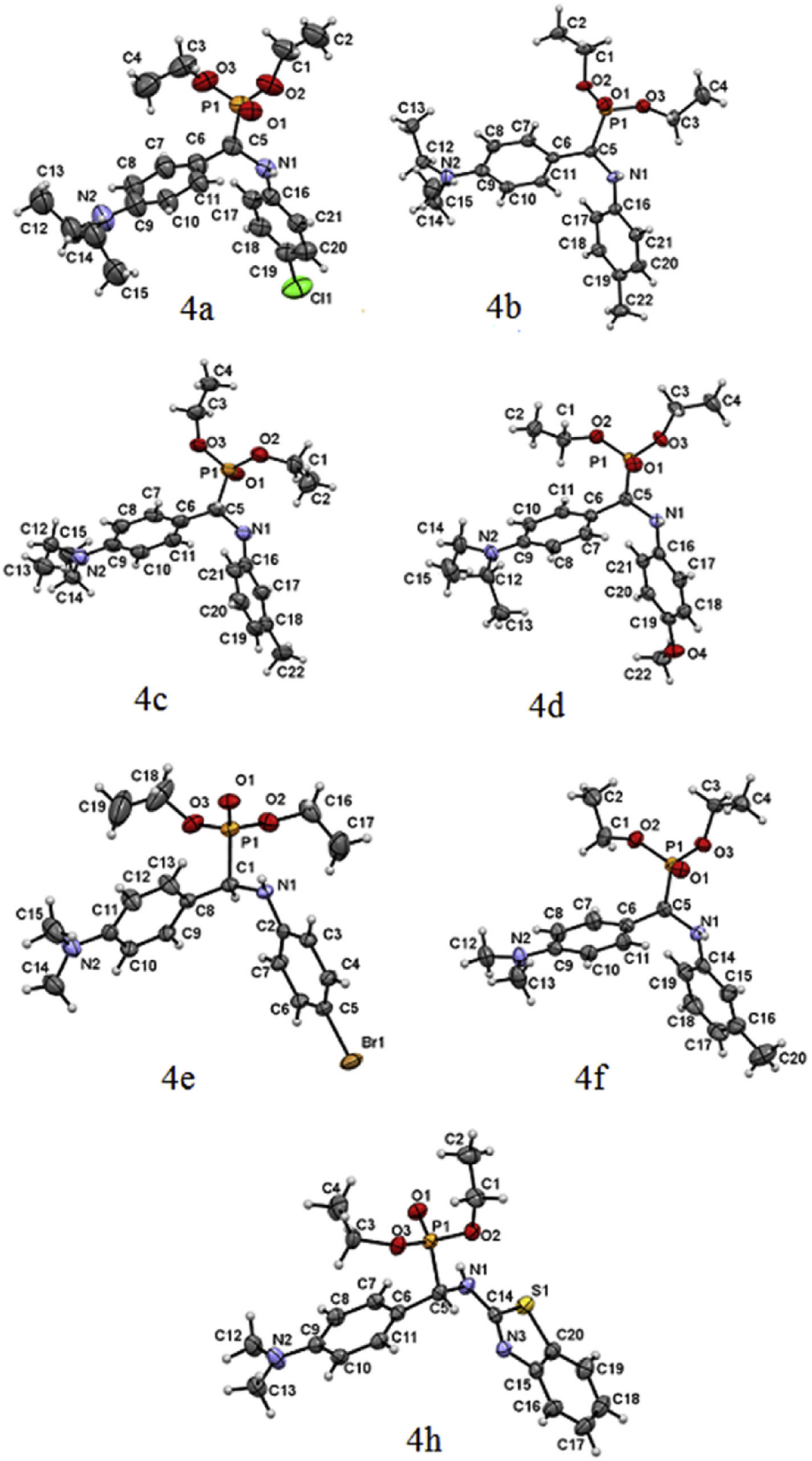

Fig. 1. Molecular structure of compounds **4a**-**4h** with the atom numbering scheme. Ellipsoids are drawn at the 30% (**4a** and **4e**) and 80% (**4b**-**4d** and **4f**-**4h**) probability level.

Table 2
The Hydrogen-Bonding Interactions present in **4a-4h**. Cg is the center of the aromatic ring.

D-H ….A(O, C, Cl, Cg)	D(D-H)/Å	d(H … A)/Å	d(D-A)/Å	D-H-A/deg
4a				
N1A-H1NA … O1B^{i}	0.892	2.88	3.045	160.81
N1B–H1B···O1A^{i}	0.900	2.009	2.904	172.35
C11B–H11B···O1A^{i}	0.931	2.667	3.427	139.31
C21A-H21A … O1B^{i}	0.93	2.546	3.295	137.76
C4B–H4BA … Cl1B^{i}	0.961	2.61	3.453	146.59
C21B–H21B ….π(Cg1)	0.930	3.660	4.528	156.41
C4B–H4BC ….π(Cg2)	0.959	3.976	4.888	159.78
4b			2.546	
N1–H1N···O1 ^{ii}	0.893	2.038	2.929	175.69
C2–H2C···O1 ^{iii}	0.960	2.674	3.502	144.73
C8–H8 ….π(Cg1)	0.930	3.777	4.599	149.02
4c				
N1–H1N···O1 ^{iv}	0.895	2.154	3.037	168.69
C17–H17···O1 ^{iv}	0.93	2.668	3.379	133.86
C11–H11···O1 ^{iv}	0.93	2.572	3.485	167.31
C3–H3A ….π(Cg1)	0.957	2.722	3.600	152.76
4d				
N1A-H1NA-O1A^{v}	0.886	2.344	3.199	162.20
C21A-H21A … O1A^{v}	0.930	2.460	3.289	148.52
N1B–H1NB...O1B^{vi}	0.893	2.049	2.906	160.38
C17B–H17B···O1B^{vi}	0.930	2.489	3.169	130.11
C7B–H7B···O1B^{vi}	0.931	2.689	3.587	162.28
C5B–H5B ….π(Cg1)	0.980	3.949	4.860	155.78
C14A-H14A ….π(Cg1)	0.969	3.351	4.168	143.23
C12B–H12C ….π(Cg1)	0.970	3.562	4.286	133.34
4e				
N1–H···O1 ^{vii}	0.824	2.231	3.039	166.88
C3–H3···O1 ^{vii}	0.930	2.692	3.406	134.14
C4–H4 … π(Cg1)	0.930	3.598	4.467	156.67
4f				
N1–H1N···O1 ^{viii}	0.890	2.095	2.955	162.31
C15–H15···O1 ^{viii}	0.930	2.550	3.240	131.39
C11–H11···O1 ^{viii}	0.930	2.686	3.579	160.99
C20–H20C ….π(Cg2)	0.961	3.485	4.424	166.40
C13–H13B ….π(Cg1)	0.960	3.480	4.364	154.10
C12–H12B ….π(Cg1)	0.960	2.905	3.844	154.10
4h				
N1–H1N···O1^{v}	0.890	2.095	2.955	162.31
C13–H13B … π(Cg1)	0.961	3.429	4.024	122.21
C18–H18 ….π(Cg1)	0.930	3.343	4.164	148.43
C12–H12B … π(Cg2)	0.960	3.325	4.214	154.97
C13–H13B … π(Cg2)	0.961	2.937	4.024	151.58
C2–H2B … π(Cg2)	0.960	2.759	3.644	153.61

Symmetry codes: (i) x,y,z; (ii) 1-x,-y,-z; (iii) -x,-y,-z; (iv) 1-x,1-y,2-z; (v) 1-x,1-y,1-z; (vi) 1-x,2-y,-z; (vii) 1-x,-y,1-z; (viii) 2-x,1-y,1-z.

(inside the brackets). These differences in the geometry parameters show the existence of hydrogen bonds in the dimer structures. The comparison of these parameters (especially the H···O bond length) shows that the strength of hydrogen bond for compounds **4a**-**4h** decreases as bellow:

4h > 4e > 4a > 4c > 4f > 4b > 4d

The binding energies of the dimer structures of these compounds were quantitatively evaluated and summarized in Table 4. These binding energies are calculated by subtracting the energies of the two monomers from the dimer species. Generally, these results confirm the strength order of the hydrogen bonds mentioned above for all compounds.

3.2.2. Investigation of substituent effects on the stability and HOMO-LUMO gap

To explore the effect of the substituents on the stability of compounds **4a**-**4h**, the position of HOMO and LUMO and their energy gaps were calculated. For the simplicity, the two resonant rings are named R_1 and R_2 which corresponds to the rings coordinated to N and Cα in structures **4a**-**4f**, respectively (Scheme 2).

The surface diagrams, energy gap and the types of the HOMO and LUMO molecular orbitals for all compounds are shown in Fig. 9. It is clear from Fig. 9 that the HOMO orbital is located on the lone pair of N2 in **4a** while for the other compounds, it is located on R_1 and LUMO orbital is positioned on R_2 in all compounds. It was demonstrated that the presence of different substituents on these rings can significantly affect the HOMO-LUMO energy gaps and subsequently on the stability and activity of these compounds. Therefore, we expect different stabilities for **4a** (*p*-Cl) (4.810eV), **4b** (*p*-Me) (4.687eV) and **4d** (*p*-OCH_3) (4.535 eV) confirmed by observation of larger HOMO-LUMO energy gap for **4a** containing an electron acceptor substituent on the para-position of R_1. Not only the type but also the position of the substituent on the aromatic ring affects the stabilization energy. The presence of methyl group on the meta position of R_1 in **4c** increases the HOMO-LUMO energy gap to 4.741 eV compared to 4.687 eV for the para position in **4b** resulting in larger stability. In addition, the presence of Et_2N (**4c**) or Me_2N (**4f**) substituents in the para-position of R_2 influence the HOMO-LUMO energy gap by increasing the stabilization energy from 4.741 eV to 4.775 eV. Based on the above results, one can expect that compound **4e** which contains an electron acceptor substituent (Br) on meta position of R_1 and Me_2N on para position

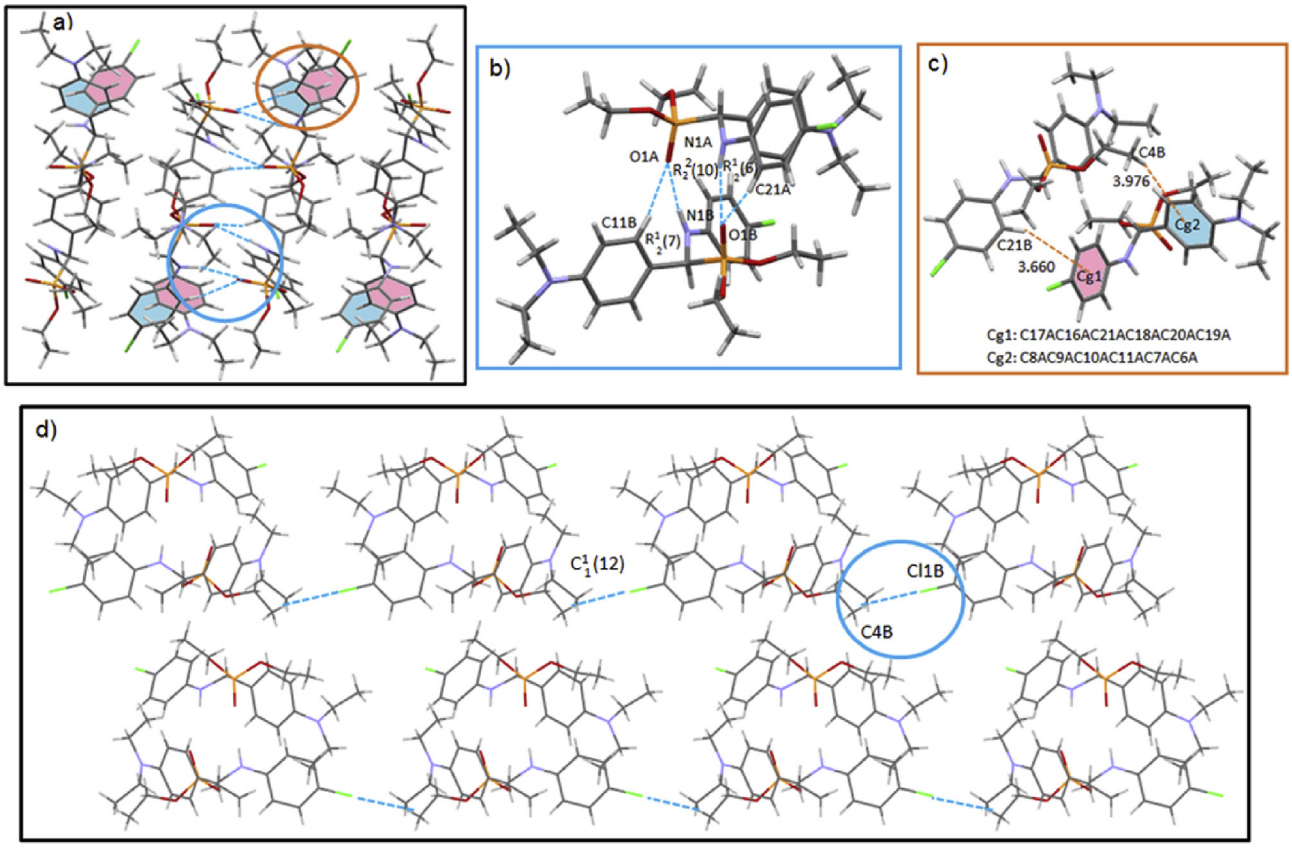

Fig. 2. a) Crystal packing of compound **4a** with indication of the hydrogen-bonding: b) NH···O, CH···O, c) CH … π and d) CH···Cl interactions and corresponding synthons.

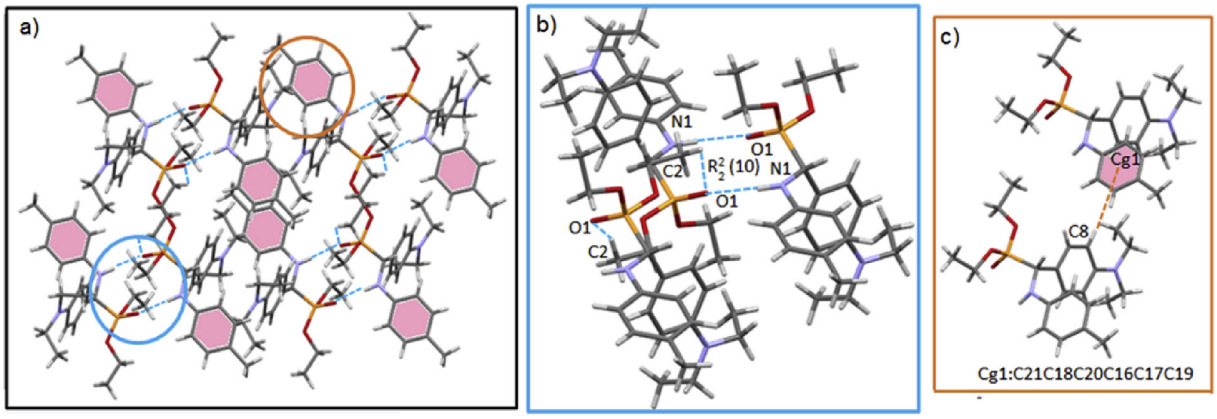

Fig. 3. a) Crystal packing of compound **4b** with indication of the hydrogen-bonding: b) NH···O, CH···O and c) CH … π interactions and corresponding synthons.

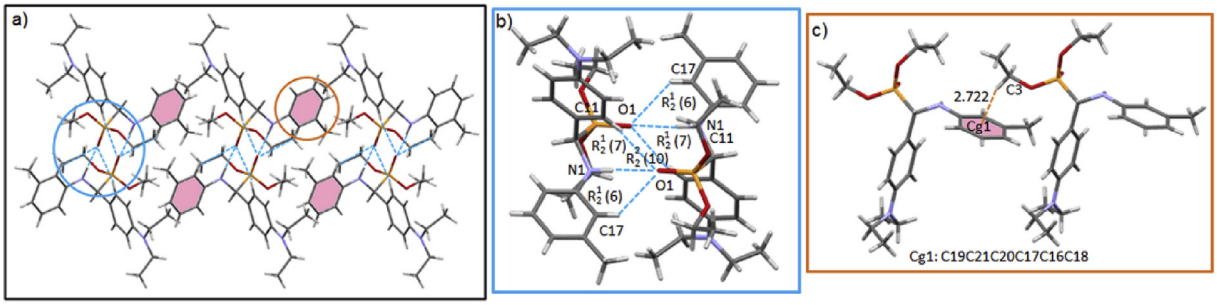

Fig. 4. a) Crystal packing of compound **4c** with indication of the hydrogen-bonding: b) NH···O, CH···O and c) CH … π interactions and corresponding synthons.

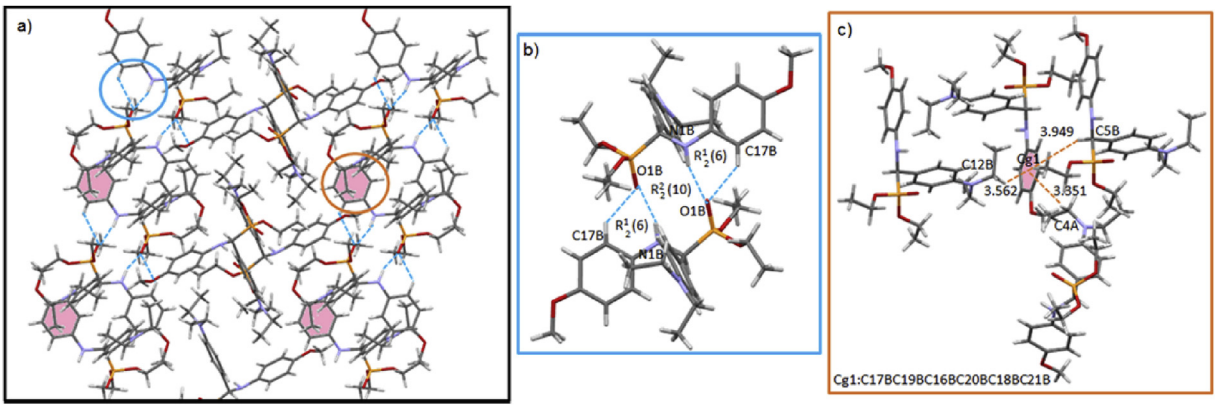

Fig. 5. a) Crystal packing of compound **4d** with indication of the hydrogen-bonding: b) NH···O, CH···O and c) CH … π interactions and corresponding synthons.

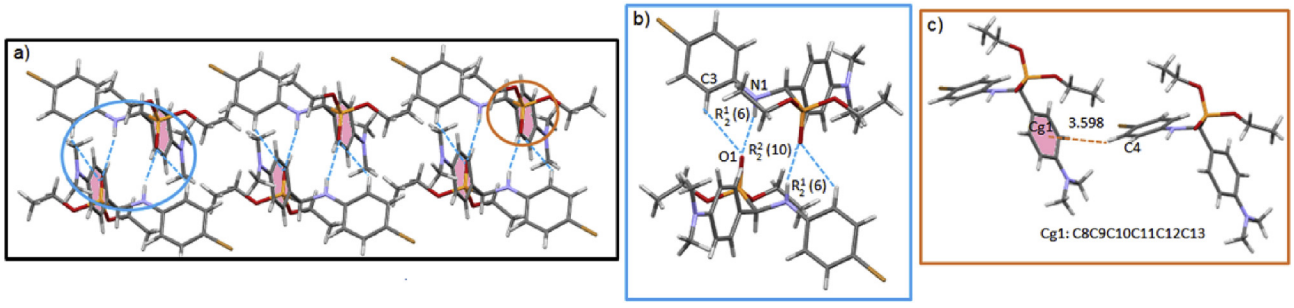

Fig. 6. a) Crystal packing of compound **4e** with indication of the hydrogen-bonding: b) NH···O, CH···O and c) CH … π interactions and corresponding synthons.

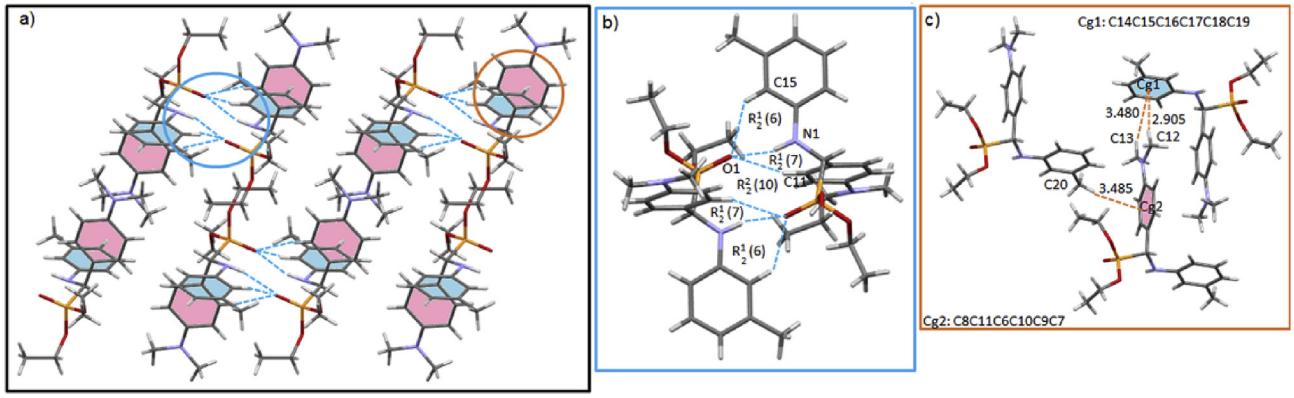

Fig. 7. a) Crystal packing of compound **4f** with indication of the hydrogen-bonding: b) NH···O, CH···O and c) CH … π interactions and corresponding synthons.

of R_2 to be the most stable compound after **4h** which is in agreement with the high energy gap of 4.825 eV. Compound **4h** has the largest stability due to the higher resonance observed in the aromatic five- and six-member rings which is in agreement with the observation of the largest HOMO-LUMO energy gap equal to 5.023 eV. In general, the large HOMO–LUMO gaps in these compounds confer high kinetic stability and low chemical reactivity since it is energetically unfavorable to add electrons to a high-lying LUMO or extract electrons from low-lying HOMO orbitals [70–72].

3.2.3. Study of hydrogen bonding by NBO analysis

The energies of the N–H···O hydrogen bonds in all structures were studied by an NBO analysis. All possible hydrogen bonds between the occupied (donor) Lewis type NBOs of oxygen and the unoccupied σ* orbitals of the N–H (acceptor) groups were considered. The energies of the interactions were estimated by the second-order perturbation theory [$E^{(2)}$]. These interactions (or energetic stabilizations) are denoted as "delocalization" corrections to the zeroth-order natural Lewis structure. A large stabilization energy $E^{(2)}$ value shows a strong interaction between an electron donor and an electron acceptor.

The results of the NBO analysis for the N–H···O hydrogen bonds are given in Table 5. The orbital energies, E, are reported in atomic units (a.u.), while the second-order perturbation energies, $E^{(2)}$, are reported in kcal mol^{-1}. The results exhibit the participation of the two lone electron pairs of the oxygen atoms (Lp(1) and Lp(2)) as donors and the σ* orbitals of the N–H groups as acceptors, with charge-transfer energy values reported in Table 5 for the hydrogen

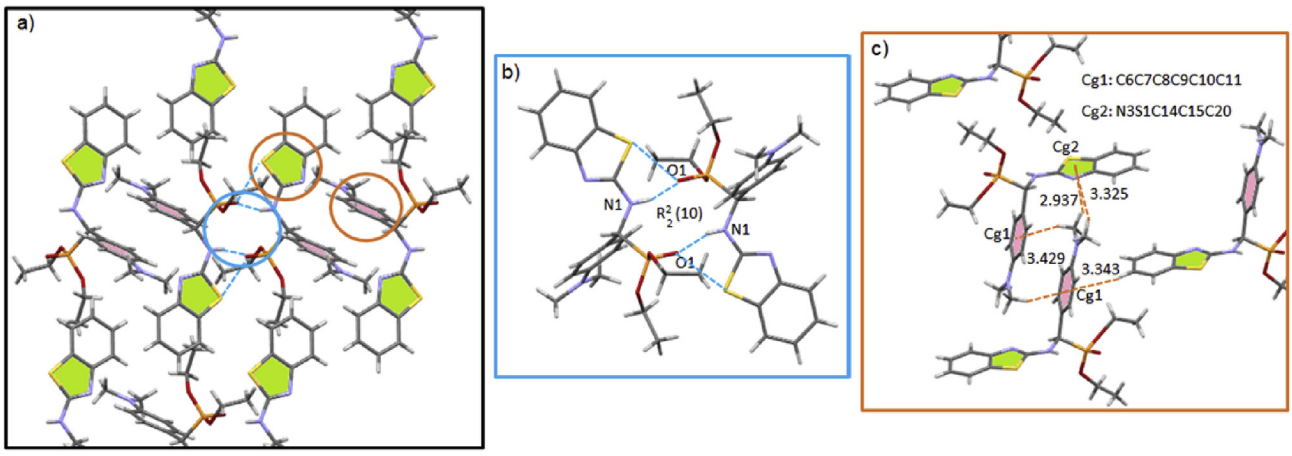

Fig. 8. a) Crystal packing of compound **4h** with indication of the hydrogen-bonding: b) NH···O and O···S and c) CH … π interactions and corresponding synthons.

Table 3
Hydrogen bonding parameters of compounds **4a**-**4h** (the data corresponding to the P═O and N–H parameters of the monomers are shown in the bracket, Bond length: Å; Bond angle: °).

Parameters	4a	4b	4c	4d	4e	4f	4h
P═O	1.493(1.485)	1.492(1.486)	1.493(1.486)	1.493(1.486)	1.493(1.485)	1.492(1.486)	1.494(1.488)
N–H	1.017(1.008)	1.017(1.009)	1.017(1.008)	1.017(1.009)	1.017(1.008)	1.017(1.008)	1.022(1.009)
H···O	1.978	1.998	1.993	2.008	1.972	1.994	1.817
N···P	4.254	4.260	4.282	4.235	4.249	4.266	4.286
NHO	161.559	162.238	163.094	160.815	161.576	162.516	175.524

Table 4
The total energy of the dimer, monomer and the binding energy of the hydrogen bonded clusters of compounds **4a**-**4h** (all energies were reported in kcal mol^{-1}).

Compound	E_{dimer}	$E_{monomer}$	$E_{binding}$
4a	−2454103.912	−1227044.674	−14.563
4b	−1926631.170	−963309.021	−13.127
4c	−1926632.213	−963309.531	−13.150
4d	−2021036.757	−1010511.811	−13.136
4e	−5008366.719	−2504175.986	−14.747
4f	−1827924.533	−913955.598	−13.338
4h	−2394158.227	−1197070.775	−16.677

bonds at the B3LYP/6-311G(d,p) level of theory. In all structures, there are two hydrogen bonds formed between N–H and oxygen atom of P═O group which is in agreement with the observation of synthon R_2^2 (10) in all structures. The surface diagram of the LpO, antibonding molecular orbitals, σ*N–H, and the resulting hydrogen bonds are illustrated in Fig. 10. The total energy $E^{(2)}$ (highlighted rows in Table 5) and the electron density of the antibonding molecular orbital, σ*N–H, for all compounds decreases in order:

4h > 4e > 4a > 4f > 4c > 4b > 4d

This order implies that the antibonding orbital with highest occupancy corresponds to the strongest hydrogen bond while the lowest occupancy is attributed to the weakest hydrogen bond. The NBO analysis shows that the maximum value of the occupancy for the antibonding orbital and the $E^{(2)}$ energy corresponds to the compound **4h** (0.07587 e and 26.45 kcal mol^{-1}), therefore, the hydrogen bond in this structure is the strongest.

Comparison of the total $E^{(2)}$ energies and HOMO-LUMO energy gaps of compounds **4a**, **4b** and **4d** reveals that the presence of electron acceptor substituent on the para position of R_1, increases the strength of the hydrogen bond. In addition, the substitution of

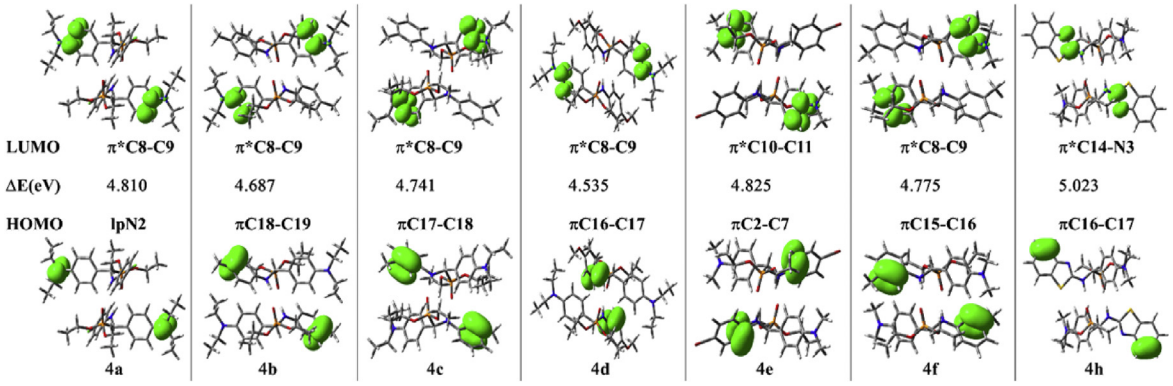

Fig. 9. Surface diagram, energy gap and the type of HOMO and LUMO for compounds **4a**-**4h**.

Table 5
NBO analysis of hydrogen bonding for all structures (Numbering according to CIF files; Occupation number: e; Energy: a.u.; $E^{(2)}$: kcal mol^{-1}).

Compounds	Donor MO			Acceptor MO			$E^{(2)}$
	Types	Occ.No.	E	Types	Occ.No.	E	
4a	Lp(1)O1A	1.96929	−0.73314	σ*N1B–H1B	0.02845	0.47097	5.29
	Lp(2)O1A	1.82452	−0.27393	σ*N1B–H1B	0.02845	0.47097	2.66
	Lp(1)O1B	1.96929	−0.73314	σ*N1A–H1B	0.02844	0.47097	5.29
	Lp(2)O1B	1.82452	−0.27393	σ*N1A–H1B	0.02844	0.47097	2.66
Summation		7.58762	−2.01414		0.05689	0.94194	15.90
4b	Lp(1)O1	1.97004	−0.7242	σ*N1–H1N	0.02739	0.48162	4.9
	Lp(2)O1	1.82402	−0.26442	σ*N1–H1N	0.02739	0.48162	2.52
	Lp(1)O1	1.97003	−0.72421	σ*N1–H1N	0.0274	0.48165	4.91
	Lp(2)O1	1.82401	−0.26443	σ*N1–H1N	0.0274	0.48165	2.53
Summation		7.5881	−1.97726		0.05479	0.96327	14.86
4c	Lp(1)O1	1.96969	−0.72433	σ*N1–H1N	0.02767	0.48191	5.13
	Lp(2)O1	1.82427	−0.26497	σ*N1–H1N	0.02767	0.48191	2.36
	Lp(1)O1	1.9697	−0.72433	σ*N1–H1N	0.02767	0.48191	5.13
	Lp(2)O1	1.82427	−0.26497	σ*N1–H1N	0.02767	0.48191	2.36
Summation		7.58793	−1.9786		0.05534	0.96382	14.98
4d	Lp(1)O1B	1.9706	−0.72355	σ*N1B–H1NB	0.02651	0.48162	4.45
	Lp(2)O1B	1.82375	−0.26311	σ*N1B–H1NB	0.02651	0.48162	2.78
	Lp(1)O1B	1.9706	−0.72355	σ*N1B–H1NB	0.02651	0.48162	4.45
	Lp(2)O1B	1.82375	−0.26311	σ*N1B–H1NB	0.02651	0.48162	2.78
Summation		7.5887	−1.97332		0.05302	0.96324	14.46
4e	Lp(1)O1	1.96907	−0.73379	σ*N1–H	0.02881	0.46987	5.43
	Lp(2)O1	1.82468	−0.27491	σ*N1–H	0.02881	0.46987	2.7
	Lp(1)O1	1.96907	−0.73379	σ*N1–H	0.02881	0.46987	5.43
	Lp(2)O1	1.82468	−0.27491	σ*N1–H	0.02881	0.46987	2.7
Summation		7.5875	−2.0174		0.05762	0.93974	16.26
4f	Lp(1)O1	1.96983	−0.72506	σ*N1–H1N	0.02763	0.48051	5.03
	Lp(2)O1	1.82409	−0.26551	σ*N1–H1N	0.02763	0.48051	2.48
	Lp(1)O1	1.96983	−0.72506	σ*N1–H1N	0.02763	0.48051	5.03
	Lp(2)O1	1.82409	−0.26551	σ*N1–H1N	0.02763	0.48051	2.48
Summation		7.58784	−1.98114		0.05526	0.96102	15.02
4h	Lp(1)O1	1.95956	−0.72936	σ*N1–H1N	0.03793	0.46747	11.54
	Lp(2)O1	1.83225	−0.27903	σ*N1–H1N	0.03793	0.46747	1.68
	Lp(1)O1	1.95953	−0.72933	σ*N1–H1N	0.03794	0.46754	11.56
	Lp(2)O1	1.83226	−0.27904	σ*N1–H1N	0.03794	0.46754	1.67
Summation		7.5836	−2.01676		0.07587	0.93501	26.45

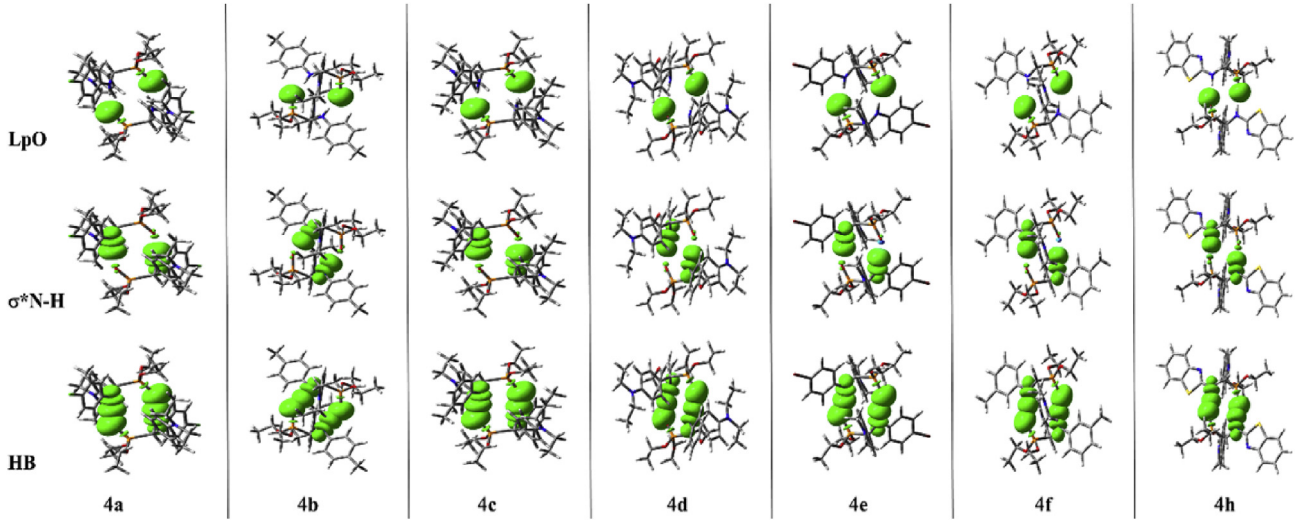

Fig. 10. Surface diagrams of LpO (top), σ*N–H (medium) and corresponding hydrogen bonds (bottom).

Et_2N group in compound **4c** by Me_2N group increases the strength of the hydrogen bond in compound **4f**. In compound **4e**, the electron acceptor substituent, Br, and Me_2N group located on para position of the R_1 and R_2 lead to the strongest hydrogen bond for this compound after **4h**.

4. Concluding remarks

The molecular and supramolecular structures of a series of synthesized α-aminophosphonates were investigated in details. All supramolecular structures indicate the characteristic α-aminophosphonate synthon R_2^2 (10) formed *via* the participating of amine and phosphonate groups in two strong NH···O═P hydrogen bonds (Scheme 1). The presence of this synthon is further confirmed by theoretical studies which revealed a higher stabilization energy for the dimer compared to the monomer. Despite of the abundant of this synthon in α-aminophosphonates, it has rarely been employed in the field of crystal engineering to synthesize supramolecular architectures and encouraged us to further explore this field. The phosphonate group has the ability to act as a simple, double or triple hydrogen acceptor and produces other synthons like R_2^1 (6) and R_2^1 (7). Accompanying conventional hydrogen bonds, unconventional hydrogen bonds including CH···O, CH···Cl and CH … π further stabilize the packing structures. These non-covalent interactions have a prominent influence on assembling the low-dimensional entities into high-dimensional supramolecular networks. The NBO analysis exhibits that the total stabilization energy $E^{(2)}$ for the NH···O hydrogen bonds in compounds **4a**-**4h** decreases in order **4h** > **4e** > **4a**>**4f** > **4c** > **4b** > **4d**. This is in excellent agreement with the HOMO-LUMO energy gaps of **4a**-**4h** which depends on the type of the substituent on the R_1 and R_2. It was demonstrated that the presence of an electron acceptor substituent and Me_2N group located on the R_1 and R_2 increase the HOMO-LUMO energy gap and stabilize the structure **4e**. However, compound **4h** with a higher degree of resonance on the aromatic ring is the most stable compound compared to the other structures.

Acknowledgements

We are grateful to Ferdowsi University of Mashhad Research Council for their financial support of this work.

Appendix A. Supplementary data

Supplementary data related to this article can be found at https://doi.org/10.1016/j.molstruc.2018.03.014.

References

[1] G.R. Desiraju, Supramolecular synthons in crystal engineering—a new organic synthesis, Angew. Chem. Int. Ed. 34 (1995) 2311–2327.
[2] E. Bosch, Role of sp-C–H…N hydrogen bonding in crystal engineering, Cryst. Growth Des. 10 (2010) 3808–3813.
[3] G.R. Desiraju, C–H···O and other weak hydrogen bonds. From crystal engineering to virtual screening, Chem. Commun. 24 (2005) 2995–3001.
[4] G.R. Desiraju, A bond by any other name, Angew. Chem. Int. Ed. 50 (2011) 52–59.
[5] M. Nishio, The CH/π hydrogen bond in chemistry. Conformation, supramolecules, optical resolution and interactions involving carbohydrates, Phys. Chem. Chem. Phys. 13 (2011) 13873–13900.
[6] O. Takahashi, Y. Kohno, M. Nishio, Relevance of weak hydrogen bonds in the conformation of organic compounds and bioconjugates: evidence from recent experimental data and high-level ab initio MO calculations, Chem. Rev. 110 (2010) 6049–6076.
[7] C.R. Martinez, B.L. Iverson, Rethinking the term “pi-stacking”, Chem. Sci. 3 (2012) 2191–2201.
[8] P. Manna, S.K. Seth, M. Mitra, A. Das, N.J. Singh, S.R. Choudhury, T. Kar, S. Mukhopadhyay, A successive layer-by-layer assembly of supramolecular frameworks driven by a novel type of face-to-face π+−π+ interactions, CrystEngComm 15 (2013) 7879–7886.
[9] S.K. Seth, P. Manna, N.J. Singh, M. Mitra, A.D. Jana, A. Das, S.R. Choudhury, T. Kar, S. Mukhopadhyay, K.S. Kim, Molecular architecture using novel types of non-covalent π-interactions involving aromatic neutrals, aromatic cations and π-anions, CrystEngComm 15 (2013) 1285–1288.
[10] S.K. Seth, D. Sarkar, T. Kar, Use of π−π forces to steer the assembly of chromone derivatives into hydrogen bonded supramolecular layers: crystal structures and hirshfeld surface analyses, CrystEngComm 13 (2011) 4528–4535.
[11] R.E. Dawson, A. Hennig, D.P. Weimann, D. Emery, V. Ravikumar, J. Montenegro, T. Takeuchi, S. Gabutti, M. Mayor, J. Mareda, Experimental evidence for the functional relevance of anion–π interactions, Nat. Chem. 2 (2010) 533–538.
[12] C. Estarellas, A. Bauzá, A. Frontera, D. Quiñonero, P.M. Deyà, On the directionality of anion–π interactions, Phys. Chem. Chem. Phys. 13 (2011) 5696–5702.
[13] A. Robertazzi, F. Krull, E.W. Knapp, P. Gamez, Recent advances in anion–π interactions, CrystEngComm 13 (2011) 3293–3300.
[14] H.G. Wallnoefer, T. Fox, K.R. Liedl, C.S. Tautermann, Dispersion dominated halogen–π interactions: energies and locations of minima, Phys. Chem. Chem. Phys. 12 (2010) 14941–14949.
[15] P. Manna, S.K. Seth, A. Bauza, M. Mitra, S. Ray Choudhury, A. Frontera, S. Mukhopadhyay, pH dependent formation of unprecedented water–bromide cluster in the bromide salts of PTP assisted by anion– π interactions: synthesis, structure, and DFT study, Cryst. Growth Des. 14 (2014) 747–755.
[16] P. Manna, S.K. Seth, A. Das, J. Hemming, R. Prendergast, M. Helliwell, S.R. Choudhury, A. Frontera, S. Mukhopadhyay, Anion induced formation of supramolecular associations involving lone pair– π and anion– π interactions in Co (II) malonate complexes: experimental observations, Hirshfeld surface analyses and DFT studies, Inorg. Chem. 51 (2012) 3557–3571.
[17] P. Manna, S.K. Seth, M. Mitra, S.R. Choudhury, A. Bauza, A. Frontera, S. Mukhopadhyay, Experimental and computational study of counterintuitive $ClO_4^-\cdots ClO_4^-$ interactions and the interplay between π+−π and Anion··· π+ interactions, Cryst. Growth Des. 14 (2014) 5812–5821.
[18] M. Mitra, P. Manna, A. Bauza, P. Ballester, S.K. Seth, S. Ray Choudhury, A. Frontera, S. Mukhopadhyay, 3-picoline mediated self-assembly of M (II)–malonate complexes (M= Ni/Co/Mn/Mg/Zn/Cu) assisted by various weak forces involving lone pair– π, π–π, and anion··· π–hole interactions, J. Phys. Chem. B 118 (2014) 14713–14726.
[19] S.K. Seth, I. Saha, C. Estarellas, A. Frontera, T. Kar, S. Mukhopadhyay, Supramolecular self-assembly of M-IDA complexes involving lone-pair··· π interactions: crystal structures, hirshfeld surface analysis, and DFT calculations [H_2IDA= iminodiacetic acid, M= Cu(II), Ni(II)], Cryst. Growth Des. 11 (2011) 3250–3265.
[20] A. Mukherjee, S. Tothadi, G.R. Desiraju, Halogen bonds in crystal engineering: like hydrogen bonds yet different, Acc. Chem. Res. 47 (2014) 2514–2524.
[21] E. Parisini, P. Metrangolo, T. Pilati, G. Resnati, G. Terraneo, Halogen bonding in halocarbon–protein complexes: a structural survey, Chem. Soc. Rev. 40 (2011) 2267–2278.
[22] P. Politzer, J.S. Murray, T. Clark, Halogen bonding and other σ-hole interactions: a perspective, Phys. Chem. Chem. Phys. 15 (2013) 11178–11189.
[23] K.E. Riley, P. Hobza, The relative roles of electrostatics and dispersion in the stabilization of halogen bonds, Phys. Chem. Chem. Phys. 15 (2013) 17742–17751.
[24] Y. Zhang, N. Ma, W. Wang, A new class of halogen bonds that avoids the σ-hole, Chem. Phys. Lett. 532 (2012) 27–30.
[25] J. Bonin, C. Costentin, M. Robert, J.M. Saveant, C.d. Tard, Hydrogen-bond relays in concerted proton–electron transfers, Acc. Chem. Res. 45 (2011) 372–381.
[26] E.D. Głowacki, M. Irimia-Vladu, S. Bauer, N.S. Sariciftci, Hydrogen-bonds in molecular solids–from biological systems to organic electronics, J. Mater. Chem. B 1 (2013) 3742–3753.
[27] G.A. Jeffrey, W. Saenger, Hydrogen Bonding in Biological Structures, Springer Science & Business Media, 2012.
[28] B. Moulton, M.J. Zaworotko, From molecules to crystal engineering: supramolecular isomerism and polymorphism in network solids, Chem. Rev. 101 (2001) 1629–1658.
[29] J. Bernstein, R.E. Davis, L. Shimoni, N.L. Chang, Patterns in hydrogen bonding: functionality and graph set analysis in crystals, Angew. Chem. Int. Ed. 34 (1995) 1555–1573.
[30] S.K. Seth, Tuning the formation of MOFs by pH influence: X-ray structural variations and Hirshfeld surface analyses of 2-amino-5-nitropyridine with cadmium chloride, CrystEngComm 15 (2013) 1772–1781.
[31] S.K. Seth, A. Bauzá, A. Frontera, Screening polymorphism in a Ni (ii) metal–organic framework: experimental observations, Hirshfeld surface analyses and DFT studies, CrystEngComm 20 (2018) 746–754.
[32] S.K. Seth, D. Sarkar, A.D. Jana, T. Kar, On the possibility of tuning molecular edges to direct supramolecular self-assembly in coumarin derivatives through cooperative weak forces: crystallographic and Hirshfeld surface analyses, Cryst. Growth Des. 11 (2011) 4837–4849.
[33] S.K. Seth, D. Sarkar, A. Roy, T. Kar, Insight into supramolecular self-assembly directed by weak interactions in acetophenone derivatives: crystal structures and Hirshfeld surface analyses, CrystEngComm 13 (2011) 6728–6741.
[34] S.A. Mulla, M.Y. Pathan, S.S. Chavan, S.P. Gample, D. Sarkar, Highly efficient one-pot multi-component synthesis of α-aminophosphonates and bis-α-aminophosphonates catalyzed by heterogeneous reusable silica supported

dodecatungstophosphoric acid (DTP/SiO 2) at ambient temperature and their antitubercular evaluation against Mycobactrium Tuberculosis, RSC Adv. 4 (2014) 7666–7672.
[35] A. Chrostowska, C. Darrigan, S. Khayar, P. Baylere, J. Lewkowski, A. Krzyczmonik, P. Tokarz, K. Ślepokura, T. Lis, Diastereoselective synthesis of tetraalkyl (R, R)-1, 2-cyclohexylene-diamino-di-phosphonates bearing thiophene, furan and pyrrole moieties. Computational and experimental study on their formation, Tetrahedron 71 (2015) 2561–2571.
[36] J. Lewkowski, P. Tokarz, T. Lis, K. Ślepokura, Synthesis and resolution of diastereomers of (R,R)-1,2-cyclohexylenediamino-di-phenylmethylphosphonates, Tetrahedron Asymmetry 23 (2012) 482–488.
[37] A. Mucha, P. Kafarski, L. Berlicki, Remarkable potential of the α-aminophosphonate/phosphinate structural motif in medicinal chemistry, J. Med. Chem. 54 (2011) 5955–5980.
[38] Q. Wang, L. Yang, H. Ding, X. Chen, H. Wang, X. Tang, Synthesis, X-ray crystal structure, DNA/protein binding and cytotoxicity studies of five α-aminophosphonate N-derivatives, Bioorg. Chem. 69 (2016) 132–139.
[39] H.A.L. El-Boraey, A.A.A. El-Gokha, I.E.T. El-Sayed, M.A. Azzam, Transition metal complexes of α-aminophosphonates Part I: synthesis, spectroscopic characterization, and in vitro anticancer activity of copper (II) complexes of α-aminophosphonates, Med. Chem. Res. 24 (2015) 2142–2153.
[40] K.B. Huang, Z.F. Chen, Y.C. Liu, Z.Q. Li, J.H. Wei, M. Wang, X.L. Xie, H. Liang, Platinum (II) complexes containing aminophosphonate esters: synthesis, characterization, cytotoxicity and action mechanism, Eur. J. Med. Chem. 64 (2013) 554–561.
[41] T. Kiss, J. Balla, G. Nagy, H. Kozłowski, J. Kowalik, Complexes of aminophosphonates. I. Transition metal complexes of aminophosphonic acid analogues of α-alanine, β-alanine, phenylalanine and tyrosine, Inorg. Chim. Acta. 138 (1987) 25–30.
[42] B. Żurowska, K. Ślepokura, U. Kalinowska-Lis, B. Boduszek, Synthesis, spectroscopy and magnetic properties of transition-metal complexes with diethyl [(n-butylamino-N)(pyridin-2-yl)] methylphosphonate (2-pmape): structure of $[Co(2\text{-pmape})_2](ClO_4)_2$ complex, Inorg. Chim. Acta. 348 (2012) 143–148.
[43] P. Kafarski, B. Lejczak, Biological activity of aminophosphonic acids, Phosphorus, Sulfur Silicon Relat. Elem. 63 (1991) 193–215.
[44] P. Kafarski, B. Lejczak, Aminophosphonic acids of potential medical importance, Curr. Med. Chem. Anticanc. Agents 1 (2001) 301–312.
[45] B. Lejczak, P. Kafarski, J. Zygmunt, Inhibition of aminopeptidases by aminophosphonates, Biochemistry 28 (1989) 3549–3555.
[46] D.J. Burkhart, B. Twamley, N.R. Natale, A new direct synthesis of ACPA and novel AMPA analogues, Tetrahedron Lett. 42 (2001) 8415–8418.
[47] S.L. Cockroft, C.A. Hunter, Chemical double-mutant cycles: dissecting noncovalent interactions, Chem. Soc. Rev. 36 (2007) 172–188.
[48] S. Komeda, T. Moulaei, K.K. Woods, M. Chikuma, N.P. Farrell, L.D. Williams, A third mode of DNA binding: phosphate clamps by a polynuclear platinum complex, J. Am. Chem. Soc. 128 (2006) 16092–16103.
[49] W. Saenger, G. Jeffrey, Hydrogen Bonding in Biological Structures, Springer-Verlag, Berlin, 1991.
[50] S. Bilge, S.J. Coles, D.B. Davies, M.B. Hursthouse, Z. Kılıç, J.S. Rutherford, R.A. Shaw, Clathrate and channel inclusion systems co-exist in the crystal structure of a bis-C-pivot macrocycle (Z′= 2), CrystEngComm 10 (2008) 873–878.
[51] C.N. Rao, Basic building units, self-assembly and crystallization in the formation of complex inorganic open architectures, J. Chem. Sci. 113 (2001) 363–374.
[52] B. Vahdani Alviri, M. Pourayoubi, A. Saneei, M. Keikha, A. Van Der Lee, A. Crochet, A.A. Ajees, M. Nečas, K.M. Fromm, K. Damodaran, Puckering behavior in six new phosphoric triamides containing aliphatic six-and seven-membered ring groups and a database survey of analogous ring-containing structures, Tetrahedron 74 (2018) 28–41.
[53] M. Mirzaei, H. Eshghi, M. Rahimizadeh, M. Bakavoli, M.M. Matin, M. Hosseinymehr, H.A. Rudbari, G. Bruno, An eco-friendly three component manifold for the synthesis of α-aminophosphonates under catalyst and solvent-free conditions, X-ray characterization and their evaluation as anticancer agents, J. Chin. Chem. Soc. 62 (2015) 1087–1096.
[54] M.C. Burla, R. Caliandro, M. Camalli, B. Carrozzini, G.L. Cascarano, C. Giacovazzo, M. Mallamo, A. Mazzone, G. Polidori, R. Spagna, SIR2011: a new package for crystal structure determination and refinement, J. Appl. Crystallogr. 45 (2012) 357–361.
[55] G.M. Sheldrick, SHELXS97, Program for the Solution of Crystal Structures, University of Gottingen, Germany, 1997, p. 8.
[56] G.M. Sheldrick, SHELXL-2014, Program for Structure Refinement, Universität of Göttingen, Göttingen, 2014.
[57] G.M. Sheldrick, SHELXL-97, Program for Crystal-structure Refinement, University of Gottingen, Germany, 1997.
[58] M. Frisch, G. Trucks, H.B. Schlegel, G. Scuseria, M. Robb, J. Cheeseman, G. Scalmani, V. Barone, B. Mennucci, G. Petersson, Gaussian 09, Revision a. 02, gaussian. Inc., Wallingford, CT, 2009, p. 200.
[59] E. Glendening, A. Reed, J. Carpenter, F. Weinhold, NBO, Version 3.1. 44 RFW Bader. Atoms in Molecules: a Quantum Theory, 2003.
[60] F. Hamzehee, M. Pourayoubi, A. Farhadipour, D. Choquesillo-Lazarte, Two new phosphinic amides: synthesis, crystal structure, and theoretical study of hydrogen bonding, Phosphorus, Sulfur Silicon Relat. Elem. 192 (2017) 359–367.
[61] F. Sabbaghi, M. Pourayoubi, A. Farhadipour, N. Ghorbanian, P.V. Andreev, A novel tubular hydrogen-bond pattern in a new diazaphosphole oxide: a combination of X-ray crystallography and theoretical study of hydrogen bonds, Acta Crystallogr. Sect. C Struct Chem. 73 (2017) 569–574.
[62] C.F. Macrae, I.J. Bruno, J.A. Chisholm, P.R. Edgington, P. McCabe, E. Pidcock, L. Rodriguez-Monge, R. Taylor, J. v. Streek, P.A. Wood, Mercury CSD 2.0–new features for the visualization and investigation of crystal structures, J. Appl. Crystallogr. 41 (2008) 466–470.
[63] M. Krishnaiah, V. Surendra Babu, G. Syam Prasad, C. Suresh Reddy, V.G. Puranik, Diethyl [(5-chloro-2-hydroxyanilino)(4-chlorophenyl) methyl] phosphonate, Acta Crystallogr. E Struct. Rep. Online 65 (2009) o2506–o2507.
[64] X. Wang, Y. Cai, J. Chen, F. Verpoort, A simple protocol for the synthesis of α-substituted phosphonates, Phosphorus, Sulfur Silicon Relat. Elem. 191 (2016) 1268–1273.
[65] M.X. Li, M.L. Zhu, L.P. Lu, Ethyl [(2-hydroxyphenyl)(pyridinium-2-ylamino) methyl] phosphonate methanol solvate, Acta Crystallogr. E: Struct. Rep. Online 64 (2008) o1178–o1179.
[66] I. Kraicheva, I. Tsacheva, E. Vodenicharova, E. Tashev, K. Troev, rac-Dimethyl [(9-anthryl)(4-methylanilino) methyl] phosphonate, Acta Crystallogr. E: Struct. Rep. Online 67 (2011) o2045–o2045.
[67] S. Kumar, S.C. Taneja, M.S. Hundal, K.K. Kapoor, One-pot synthesis of α-aminophosphonates catalyzed by antimony trichloride adsorbed on alumina, Tetrahedron Lett. 49 (2008) 2208–2212.
[68] Y.P. Hong, B.-A. Song, X.-C. Shangguan, Dimethyl [(4-fluorophenyl)(6-methoxybenzothiazol-2-ylamino) methyl] phosphonate, Acta Crystallogr. E: Struct. Rep. Online 65 (2009) o1199–o1200.
[69] I.A. Tayubi, R. Sethumadhavan, Theoretical understanding of CH.... π interactions and their distribution in immunoglobulin proteins insilco geometrical approach, Int. J. Pharm. Pharmaceut. Sci. 3 (2011) 212–218.
[70] S.K. Seth, S. Banerjee, T. Kar, Crystal structure and DFT calculations of andrographiside, J. Mol. Struct. 965 (2010) 45–49.
[71] S.K. Seth, G.C. Maity, T. Kar, Structural elucidation, Hirshfeld surface analysis and quantum mechanical study of para-nitro benzylidene methyl arjunolate, J. Mol. Struct. 1000 (2011) 120–126.
[72] S.K. Seth, N.C. Saha, S. Ghosh, T. Kar, Structural elucidation and electronic properties of two pyrazole derivatives: a combined X-ray, Hirshfeld surface analyses and quantum mechanical study, Chem. Phys. Lett. 506 (2011) 309–314.